Modelling of loading, stress relaxation and stress recovery in a shape memory polymer

J. Sweeney[a], M. Bonner[b], I.M. Ward[b]

[a] IRC in Polymer Science and Technology, School of Engineering and Informatics, University of Bradford, Bradford BD7 1DP,UK
[b] IRC in Polymer Science and Technology, School of Physics & Astronomy, The University of Leeds, Leeds LS2 9JT, UK

Abstract

A multi-element constitutive model for a lactide-based shape memory polymer has been developed that represents loading to large tensile deformations, stress relaxation and stress recovery at 60, 65 and 70°C. The model consists of parallel Maxwell arms each comprising neo-Hookean and Eyring elements. Guiu-Pratt analysis of the stress relaxation curves yields Eyring parameters. When these parameters are used to define the Eyring process in a single Maxwell arm, the resulting model yields at too low a stress, but gives good predictions for longer times. Stress dip tests show a very stiff response on unloading by a small strain decrement. This would create an unrealistically high stress on loading to large strain if it were modelled by an elastic element. Instead it is modelled by an Eyring process operating via a flow rule that introduces strain hardening after yield. When this process is incorporated into a second parallel Maxwell arm, there results a model that fully represents both stress relaxation and stress dip tests at 60°C. At higher temperatures a third arm is required for valid predictions.

Keywords: Shape memory; mechanical properties; constitutive modelling; modelling.

Introduction

Shape memory polymers have received considerable attention in recent years since their introduction in the 1980s. The materials and the range of applications have been reviewed by Ratna and Karger-Kocsis [1]. A shape memory polymer is created by inducing molecular chain orientation into a material; the orientation is frozen in, and may be released at a later time in response to a physical trigger, usually an increase in temperature, at which point the material reverts to its shape before orientation. These materials are finding increasing application in medical areas, where they have a number of advantages over devices made from shape memory metals. These include their ability to be triggered or activated at relatively low temperatures; their biocompatibility; the possibility of being bioresorbable, so that once their purpose has been fulfilled they do not need to be surgically removed; and the potential for dual use as drug delivery systems. Lendlein and Behl [2] have reviewed the area. Recent examples of applications have been in stents [3-6] and in a tissue engineering scaffold [7].

The material of this paper consists of a bioresorbable polymer compounded with calcium carbonate ($CaCO_3$) powder. $CaCO_3$ has been shown to be effective in improving thermal stability when mixed with PLA [8]. Also significant in the present context is its effect in controlling the rate of polymer degradation, as demonstrated when compounded with biodegradable polyurethane shape memory

biopolymers [9] to produce materials for which the rate of hydrolytic degradation depends on the filler level. This gives potential for control of the rate of resorption of an implanted device.

Typically a shape memory device will be triggered to undergo shape change by attaining a specific reversion temperature, which will be related to the temperature at which the molecular orientation was originally imposed. For implant materials, there is clearly an upper limit to the reversion temperature, depending on the specific application, so that significant tissue damage is avoided. This issue has been discussed by Gall et al. [10] who report two broad approaches: the development of materials with reversion temperatures around 37°C, so that the body's internal energy triggers the device and no external heat source is necessary; and higher reversion temperatures, for which external energy is required. In the latter case, in which local heating may be applied in bursts to minimise exposure to high temperatures, there are advantages over the former approach in that it makes available implant devices that are both mechanically stiffer and lack the need for low temperature storage. Which of the two approaches is adopted is a design decision. Gall et al. developed biomedical shape memory polymers with a glass transition temperature of 65°C, and reversion temperatures of the same order. Recently work has been undertaken to extend the range of devices that shape memory polymers can be used with by using the shape memory polymer as a part of a fixation device [11-13]. When considering materials for a fixation device such as an intramedullary nail, then materials with a T_g above 50°C are preferable since current devices are entirely metallic and do not require temperature control that is any more demanding than an air conditioned room (which is especially useful within the operating theatre), and thus adoption by surgeons would potentially be faster. These devices are also designed for use in areas of the body which are less sensitive to damage by elevated temperature, and thus temperatures in the range of 60°C can be tolerated for short periods of time. This issue should be viewed in the context of the routine use of PMMA bone cements in hip and knee replacement surgery, in which temperatures in the cement may be in excess of 70°C on polymerisation [14].

Once an implant has been installed and activated, it is desirable that the development with time of the recovered shape and forces acting on it be predictable at the design stage. As pointed out by Nguyen et al. [15], this requires numerical modelling, which itself requires a validated constitutive equation, the subject of this paper. A validated numerical model of a device will also predict the duration of time at which it needs to be held at the triggering temperature, to assist in the design issue discussed above. While the shape memory process in polymers is associated with temperature change, an understanding of isothermal behaviour is a prerequisite for developing an appropriate constitutive model. Recovery phenomena can be observed isothermally, and their understanding provides a key for the modelling of shape recovery. They can be accessed via stress dip tests. These exploit the observation that, when a polymer specimen is strained in tension and then partially unloaded to a constant lower strain, the stress, which remains tensile, may subsequently increase, or recover, with time. Since the total strain energy can only decrease, stress recovery is explicable by there being a component of the total stress that is compressive. When modelling the material using mechanical (e.g. spring-and-dashpot) networks, this can be represented by including at least two parallel arms, so that one arm is in tension while the other one is in compression. Whenever stress recovery is observed, it is thus implied that the representation must include two or more parallel arms.

Depending on the level of strain unloading, on its completion the stress may relax, (for small levels of unloading), recover (at higher levels) or, at an intermediate level, remain initially constant. The stress level in this last case was a subject of major importance in a classic study by Fotheringham and Cherry [16] of linear polyethylene, in which partial unloading was carried out in a series of stress dip tests and these three responses were studied. The responses were interpreted in spring-and-dashpot terms as a model consisting of two parallel arms, one arm being associated with an internal or recovery stress and the other with an Eyring process. The response of constant recovery stress was associated with there being zero stress in the Eyring arm; the recovery stress was then equated with the total applied stress, and its dependence on strain and strain rate analysed, leading to a quantitative understanding of the material model.

Strain or shape recovery is a closely related phenomenon, and is of particular significance for shape memory polymers. When subject to zero total stress, a two-arm model in which one arm is in tension with elastic stored energy will contract, with consequent compression of the other arm. If the other arm has viscous properties, the unloading process will take time to reach equilibrium - the recovery time - and this quantity is of interest for the development of shape memory materials. Recently Bonner et al. [17] reported a simple method for predicting the recovery time for a shape memory polymer intended for medical applications. The method was based on the use of such a two-arm model, which took the form of a linear viscoelastic Kelvin-Voigt model. Transient stress dip tests, in which specimens were drawn up to a ratio of 4 and then unloaded by a small strain, were carried out in tension at temperatures in the range 55 - 75°C. These tests provided data to predict the recovery time of the drawn specimens, reheated to temperatures close to the drawing temperatures, under creep conditions. Successful predictions of the recovery time were made using this model and procedure.

While the success of the work described above on both stress and shape recovery has shown the utility of the Kelvin-Voigt representation, it is important to note that in both cases the modelling was initiated from a state of stress and strain corresponding to that at the start of the stress dip. While the model parameters derived are fit for the purpose of predicting the subsequent behaviour, they are not necessarily valid more generally. It is likely that that, if the same model were loaded from an initial state of zero stress and strain up to the strain just preceding the stress dip, the stress would not correspond to that observed. This is similar to the situation we describe below, where a single-arm model, with parameters that have been fitted using a stress relaxation test, yields before the stress reaches that observed in stress relaxation (Figure 4). If we are to implement the findings that arise from stress dip experiments, for instance by incorporating them in a finite element analysis, then we need a constitutive model that is valid from the initial state of zero stress and strain. Such a model is the subject of this paper.

In this programme of research on a shape memory polymer, we have made use of parallel arm models that incorporate Eyring processes and hyperelastic networks, which are implemented numerically. The models comprise either two or three parallel arms, depending on temperature. Both stress relaxation tests and stress dip experiments are used to derive parameter values. In the stress dip experiments, unlike Fotheringham and Cherry, we do not seek the unloading level that results in constant stress; rather, we consider it sufficient to use the model's numerical implementation to predict the behaviour resulting from both small and large strain dips. The analysis

of Guiu and Pratt [18] is generalised to large strains and used to analyse stress relaxation curves and derive Eyring parameters. In order for a single model to be capable of modelling both loading and stress dip behaviour, it is found that the observed very high stiffness of response in unloading could only be made compatible with the stress levels during loading by a strain dependent Eyring process; this is achieved by the application of an appropriate flow rule that depends on the material's evolving anisotropy. The use of step dip tests has thus led to an important advance in the understanding of this material.

Materials and methods

Materials

The material is a Poly(DL-lactide-co-glycolide) containing 65% Poly-DL-Lactide and 35% polyglycolic acid, the same material as used in the study of Bonner et al. [17]. Its proposed biomedical applications are outlined in a series of patents [11-13]. It has a glass transition temperature of around 55°C. The molecular weight of the as received polymer was between 25,000 and 30,000 and varied since the polymer is a medical grade material produced in small batches. The polymer was compounded with 35wt% $CaCO_3$ on a ThermoFisher twin screw extruder. This melt processing step did cause some reduction in molecular weight, which was not quantified on a regular basis due to cost considerations. The $CaCO_3$ was added for two reasons. Firstly it acts as a buffer during degradation of the polymer in the body, helping to maintain a more neutral Ph than would occur with the pure polymer. Secondly it acts to modify the degradation rate of the polymer, making it a more usable material. Its effect on mechanical properties was not one of the motivations of this study, though on the basis of previous work on PLA/ $CaCO_3$ composites [8], there could be some small increase in the tensile strength and modulus due to the presence of this micro-sized filler.

Stress relaxation

These tests were performed using an Instron 5545 at the temperatures 60, 65 and 70°C. Specimens of length 75 mm were stretched at a constant true strain rate of 0.0167 s^{-1} to a maximum extension ratio of 4.0, and then held at constant strain for 2,500s while monitoring the stress decay.

Stress dip tests

The stress dip tests were carried out at the three test temperatures 60, 65 and 70°C using a Messphysik 20-10 tensile testing machine. Extension ratios of 4.0 were applied at a constant true strain rate of 0.0167 s^{-1} to fibre specimens of initial length 75 mm. On reaching the maximum extension they were immediately unloaded at a speed of 0.5 m min^{-1} to give a strain drop $\Delta\lambda$ of either 0.05 or 0.1, and then held at constant strain so that any stress recovery could be monitored.

Loading and stress relaxation analysis

To model the stress relaxation results and to provide the first steps towards a general constitutive model, we consider an Eyring process in series with a neo-Hookean elastic element. This latter element, also known as a Gaussian spring, is often associated with rubber elasticity and entropic stress; however, its functional form is fundamental to large deformation theory and is not unique to rubber elasticity, and in the modelling presented here we do not necessarily assume the stress arising from it to be entropic. This two element model, illustrated in Figure 1(a), provides a large deformation analogue of the Guiu-Pratt analysis of stress relaxation curves [18]. The use of this analysis will enable some of the Eyring parameters to be evaluated.

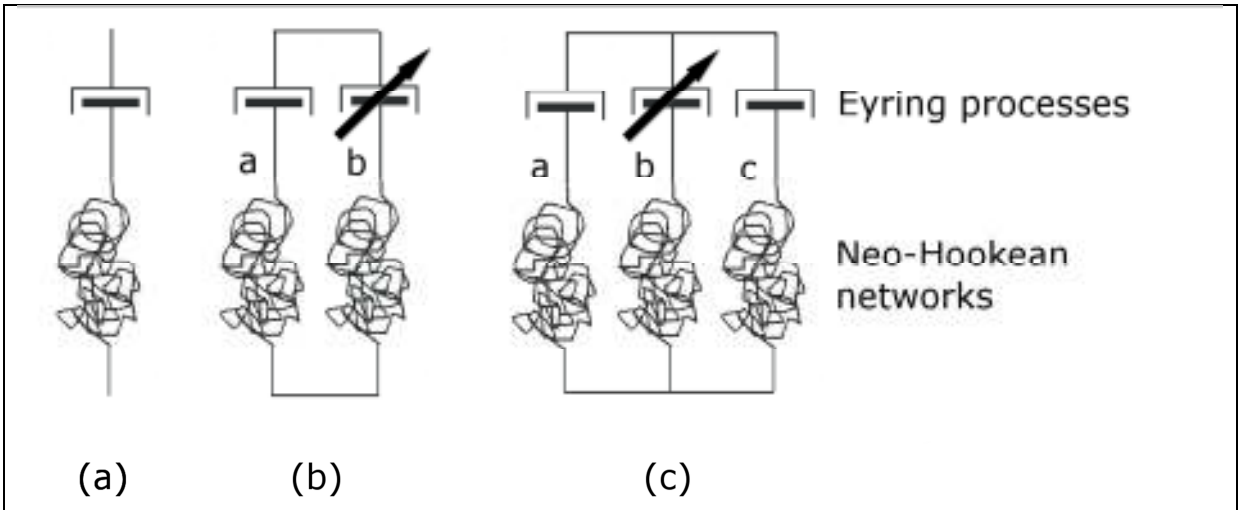

Figure 1. Development of parallel-arm constitutive models. The arrows indicate that the Eyring processes are acting in conjunction with the flow rule of equation (11), which includes strain-induced anisotropy. One-, two- and three-arm models are shown respectively in (a), (b) and (c).

The Eyring process was originally proposed by Halsey et al. [19]. In the form used here hydrostatic and shear effects are separated [20-23] to give the expression

$$\dot{e}^p = \alpha \exp\left(\frac{v_p}{kT}\bar{\sigma}\right)\sinh\left(\frac{v_s}{kT}\tau_{oct}\right) \qquad (1)$$

relating the plastic strain rate $\dot{e}^p$ to a stress tensor with octahedral shear stress τ_{oct} and mean value $\bar{\sigma}$. α is a constant pre-exponential factor and v_p and v_s are the pressure and shear activation volumes respectively, with k Boltzmann's constant and T the absolute temperature. In the following analysis for uniaxial conditions the principal directions of stress and strain remain coincident and along the global 1-2-3 axis set. For principal stresses σ_1, σ_2 and σ_3 the mean stress is given by

$$\bar{\sigma} = (\sigma_1 + \sigma_2 + \sigma_3)/3 \quad (2)$$

and the octahedral shear stress is

$$\tau_{oct} = \frac{1}{3}\left((\sigma_1 - \sigma_2)^2 + (\sigma_2 - \sigma_3)^2 + (\sigma_3 - \sigma_1)^2\right)^{1/2} (3).$$

We apply uniaxial conditions for stretching along the 1 direction and write $\sigma = \sigma_1$ and $\lambda_1^p = \lambda^p$. We introduce λ as the total extension ratio along 1 and λ_e as the elastic extension ratio in the neo-Hookean element characterised by the constant G. In the Appendix, we show that for uniaxial conditions the Maxwell model of Figure 1 (a) is characterised by

$$\frac{\dot{\lambda}}{\lambda} = \frac{\dot{\sigma}}{G\left(2(\lambda^e)^2 + 1/\lambda^e\right)} + \alpha\sqrt{2}\exp\left(\frac{v_p}{kT}\sigma/3\right)\sinh\left(\sqrt{2}\frac{v_s}{kT}\sigma/3\right) (4).$$

Also in the Appendix we show that for stress relaxation this can be approximated by

$$\frac{\dot{\sigma}}{G\left(2(\lambda^e)^2+1/\lambda^e\right)}+\frac{\alpha}{\sqrt{2}}\exp\left(\frac{v}{kT}\sigma\right)=0 \qquad (5)$$

where

$$v=\left(v_p+\sqrt{2}v_s\right)/3 \qquad (6).$$

v is of the same order as the shear activation volume v_s, and arises from the analysis of one-dimensional behaviour, sometimes being loosely referred to as "the activation volume".

Equation (5) is satisfied by a Guiu-Pratt type solution of the form

$$\sigma(t_0)-\sigma(t)=\frac{kT}{v}\ln(1+(t-t_0)/c) \qquad (7)$$

where $t > t_0$ with t_0 a fixed time, often equated to $t_0 = 0$ at the start of the stress relaxation. c is given by

$$c=\frac{kT\sqrt{2}}{\alpha v G\left(2(\lambda^e)^2+1/\lambda^e\right)}\exp\left(-\frac{v}{kT}\sigma(t_0)\right) \qquad (8).$$

In the following applications, equation (7) is fitted to stress relaxation curves to estimate V and α, and stresses during loading are calculated using a time-stepping numerical implementation of equation (4).

Loading and stress relaxation: results and initial analysis

Loading and stress relaxation data are shown for 60, 65 and 70°C are shown in Figure 2 where each result is an average of three experiments. We first make use of the stress relaxation curves to estimate Eyring parameters. Equation (6) is fitted to them using a nonlinear least squares procedure. The fitted curves are shown in Figures 3(a) – 3(c), where in

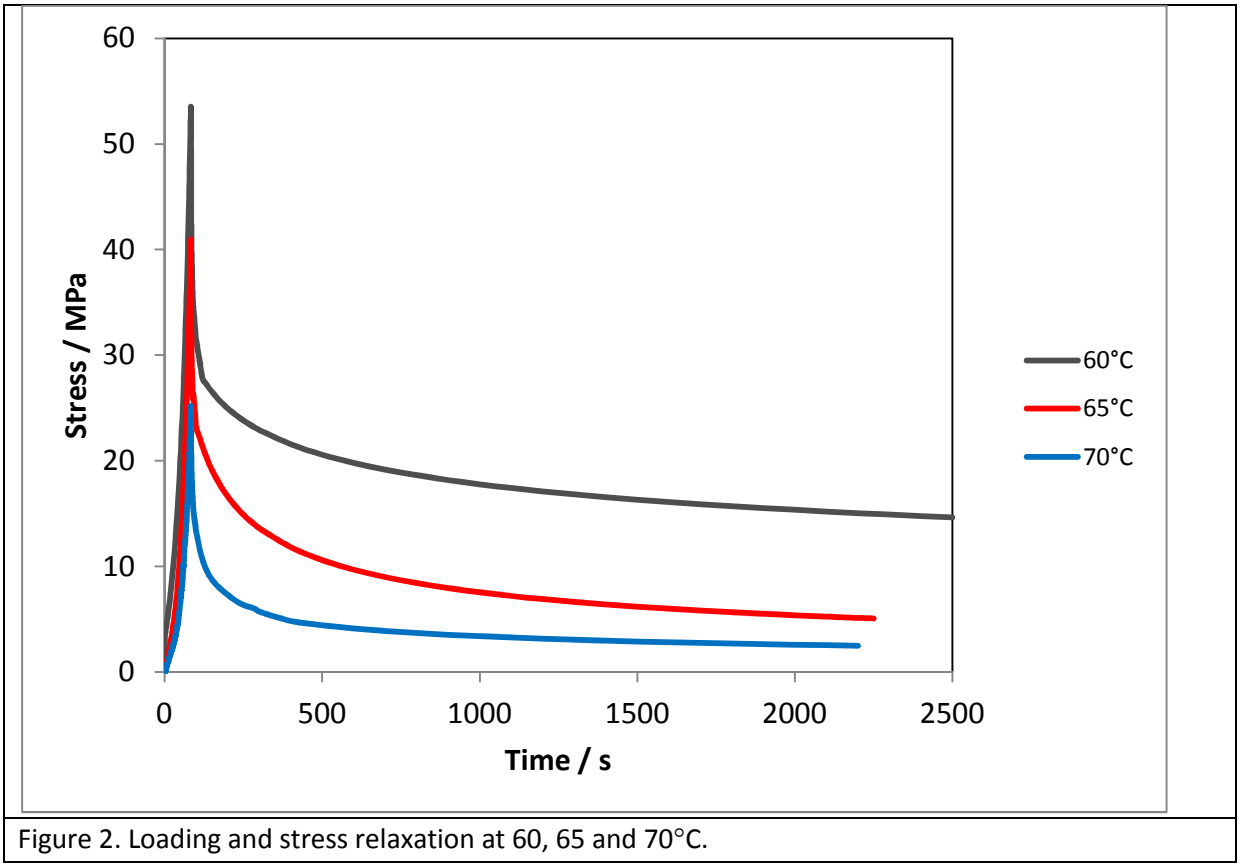

Figure 2. Loading and stress relaxation at 60, 65 and 70°C.

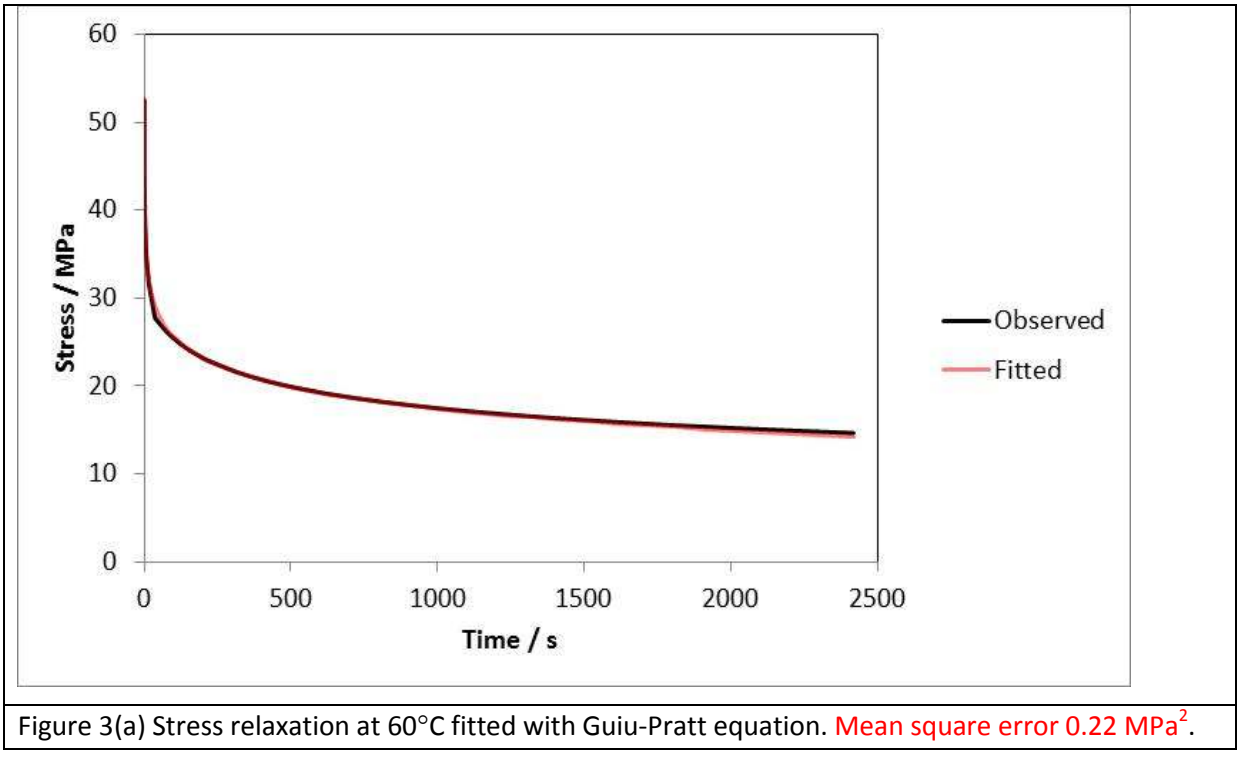

Figure 3(a) Stress relaxation at 60°C fitted with Guiu-Pratt equation. Mean square error 0.22 MPa^2.

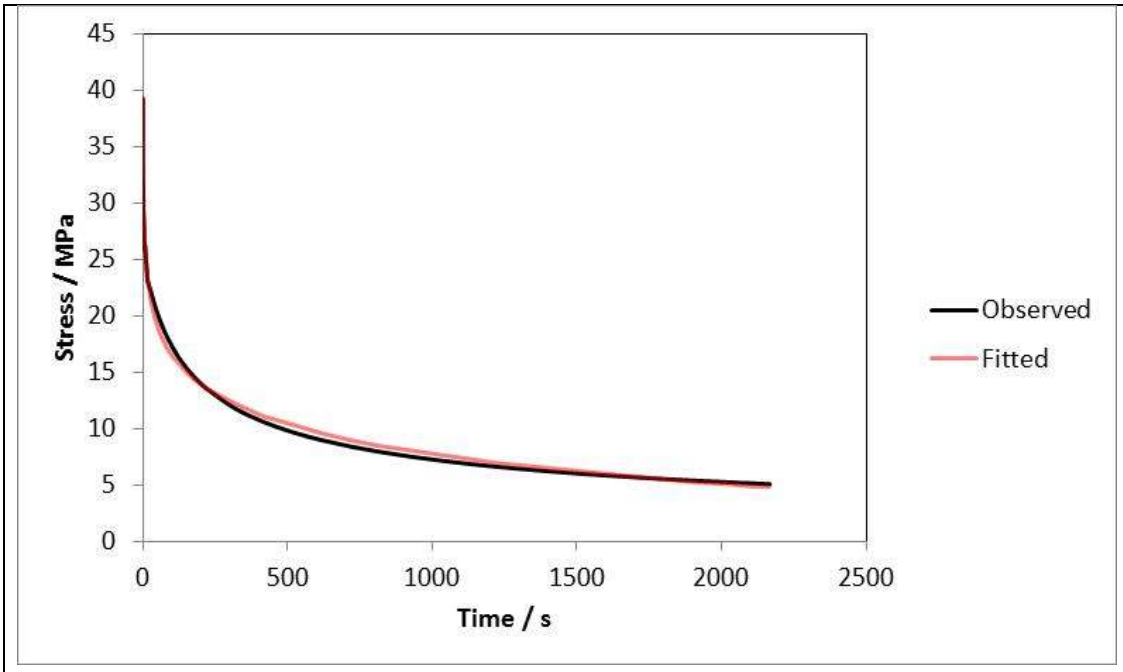

Figure 3(b) Stress relaxation at 65°C fitted with Guiu-Pratt equation. Mean square error 0.30 MPa^2.

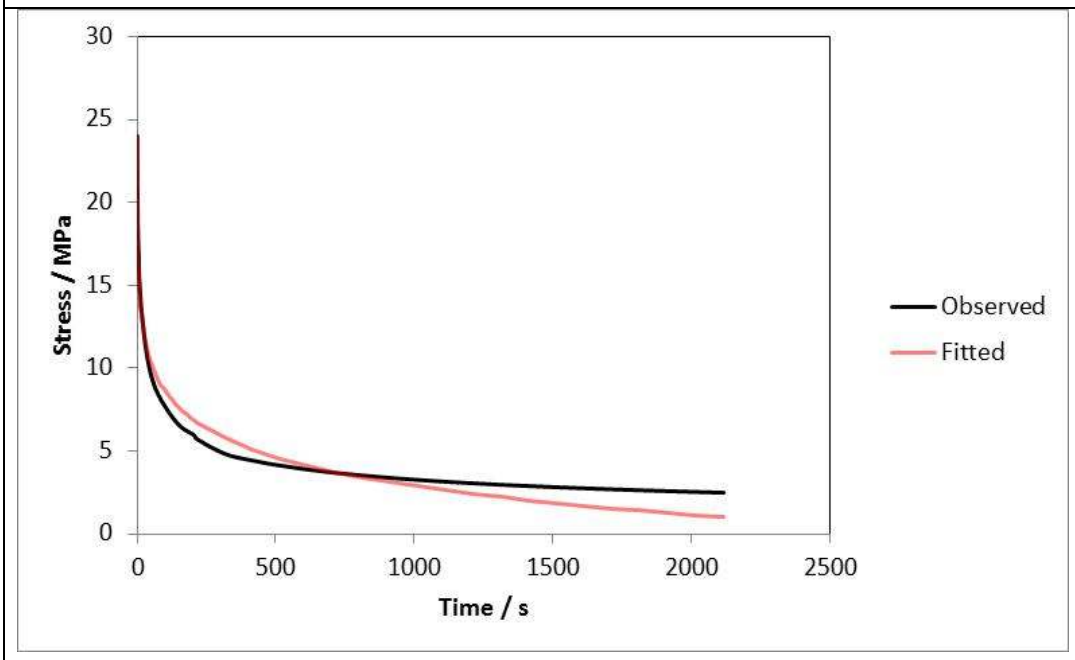

Figure 3(c) Stress relaxation at 70°C fitted with Guiu-Pratt equation. Mean square error 0.72 MPa^2.

each case the whole of the relaxation curve is fitted, with time t_0 in equation (7) taken as the start of the stress relaxation process and assigned the value $t_0 = 0$. At 60 and 65°C the fits are excellent, whereas at 70°C the fit is poor. This suggests that at this temperature the model of a single Eyring process is inadequate. However, we still make use of the fitting procedure by using non-zero values of t_0, in order to identify a time interval ($t > t_0$) where a single process is dominant. This we have done for the 70°C case using $t_0 = 200$s, as shown in Figure 3(d). This leaves open the option of adding a second parallel arm, with parameters such that its effect is to give improved predictions for times less than t_0 while contributing negligibly at times greater than t_0. This is shown to be a useful approach below, when the more general model that includes loading history is considered.

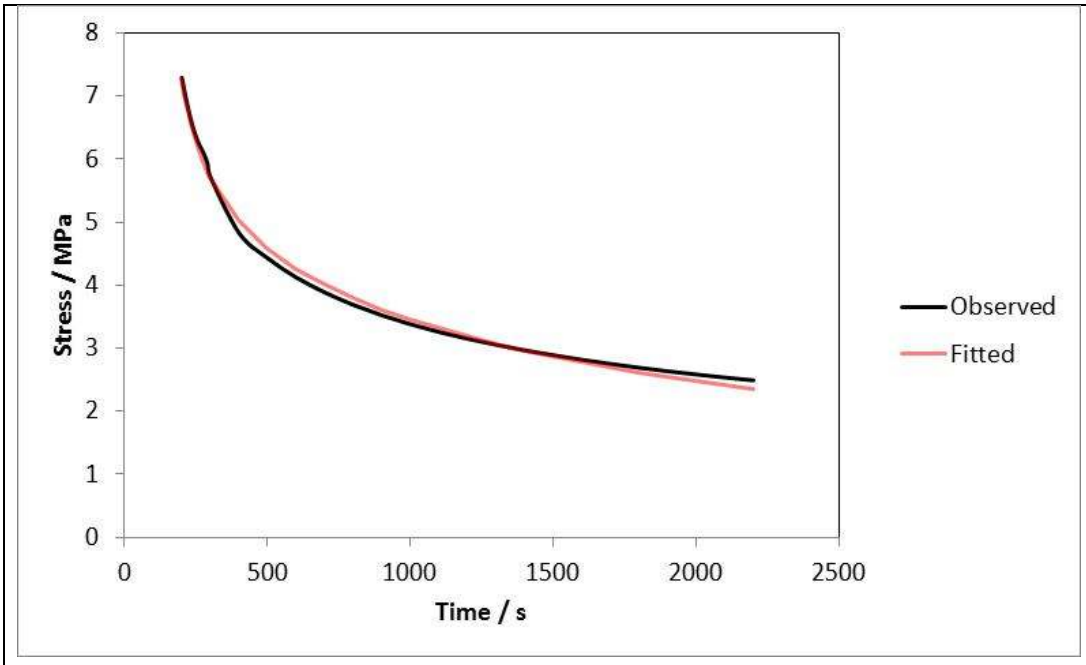

Figure 3(d) Stress relaxation at 70°C fitted with Guiu-Pratt equation from t_0 = 200s. Mean square error 0.01 MPa^2.

The values of the fitting parameters of equation (18) are given in Table 1.

Table 1 Equation (6) fitting parameters

Temperature / °C	t_0 / s	v / nm^3	c / s
60	0	1.29	0.053
65	0	1.21	0.27
70	0	1.89	0.22
70	200	3.79	39.1

The present Guiu-Pratt analysis is based on a Maxwell-type series model as shown in Figure 1(a) for which the total strain is constant. The additional assumption is that the initial state of stress and strain pertaining at t = t_0 is attainable. This assumption can be investigated by implementing numerically the model of equation (4), which is of the same Maxwell arrangement but subject to a general strain history, and applying the strain history used experimentally in the stress relaxation experiments. The experimental strain histories consist of a ramp followed by a period of constant strain as described in 'Materials and methods' above. To apply equation (4) we require the values of a number of material parameters that we derive using the results in Table 1; at 70°C we take the values fitted when t_0 = 200s.

Firstly we obtain values of v_p and v_s from the fitted values of v. We have done this using equation (6) and the relation $v_p = 0.1\ v_s$. This latter assumption is reasonably consistent with findings for a range of polymers, both semicrystalline and amorphous. Examples of values derived for v_p/v_s are 0.05 -

0.072 [24] and 0.075 [25] for polycarbonate; 0.15 for polypropylene [26]; 0.13 for ultra-high molecular weight polyethylene [27]. The consequences of varying v_p/v_s between 0.05 and 0.15 have been explored numerically and found to be slight. As a specific example, the three-arm model described below with material parameters given in Table 3 for 65°C, was loaded in tension at a strain rate of 0.0167 s^{-1}, up to an extension ratio of 4.0. Varying the value of v_p with fixed v_s gave a maximum increase in stress of 4%, occurring at the maximum strain, when v_p/v_s was decreased from 0.1 to 0.05. Similarly, increasing v_p/v_s from 0.1 to 0.15 gave a decrease in stress of 4% at the maximum strain. We conclude that the models are sufficiently insensitive to this ratio to justify the use of the fixed value of 0.1.

Table 2. Parameters for equation (15)

Temperature/ °C	v_p / nm^3	v_s / nm^3	α / s^{-1}	G / MPa	λ_e
60	0.256	2.56	7.54×10^{-7}	3.25	2.72
65	0.243	2.43	3.50×10^{-5}	2.49	1.97
70	0.748	7.48	1.3×10^{-5}	1.61	1.70

Since there is no sign of yielding during loading, we assume that there is no plastic strain on completion of loading, so that $\lambda_e = \lambda$. Then the neo-Hookean coefficient G is consistent with the stress σ_{max} at the end of loading with $\lambda_e = 4.0$. Having obtained the G value at each temperature, the values of α are related to the fitted values of c via equation (8). However, equation (8) includes λ_e, which, as noted in the Appendix, will be varying during stress relaxation and so different in value from that assumed at the beginning. We have fitted the values of α to give good prediction of stress at the end of the stress relaxation, and calculated the implied λ_e from equation (8); this is assumed to be constant according to the analysis above. The full set of parameter values for this Maxwell-like model is given in Table 2. The results at 70°C are from the t_0 = 200s results in Table 1.

The values in Tables 1 and 2 show that the activation volumes depend on temperature. It has been known for some time [28] that activation volume correlates only loosely with the size of molecular features, and may represent a sequence of co-operative mechanisms [16]. There is therefore no physical argument that would preclude temperature dependence, and it has been observed experimentally in a number of instances, for example by Strutz et al. [29].

Using the values of Table 2, stresses have been calculated using equation (4) for loading and stress relaxation at the three temperatures. The results are compared with observation in Figure 4. In all cases yield occurs in the model stress at values lower than the observed stress maxima. The assumption in our implementation of the Guiu-Pratt analysis, that the initial stress and strain is attainable by a single-arm model, is thus shown to be incorrect. However, for stress relaxation at sufficiently long times, the agreement between observation and model is good. This suggests that the stress relaxation fits have produced Eyring parameters for a process that is dominant at these

longer times, and that additional processes are required for the short time behaviour. This will be discussed below while taking into consideration the data obtained from stress dip tests, as will be the early yield at ~ 2 MPa discernible at 160°C in Figure 4(b). It should also be noted that the rationale for calculating G – that the initial stress is attained and there is no yielding – is not applicable to the model, and so the values of G for this process are as yet not defined.

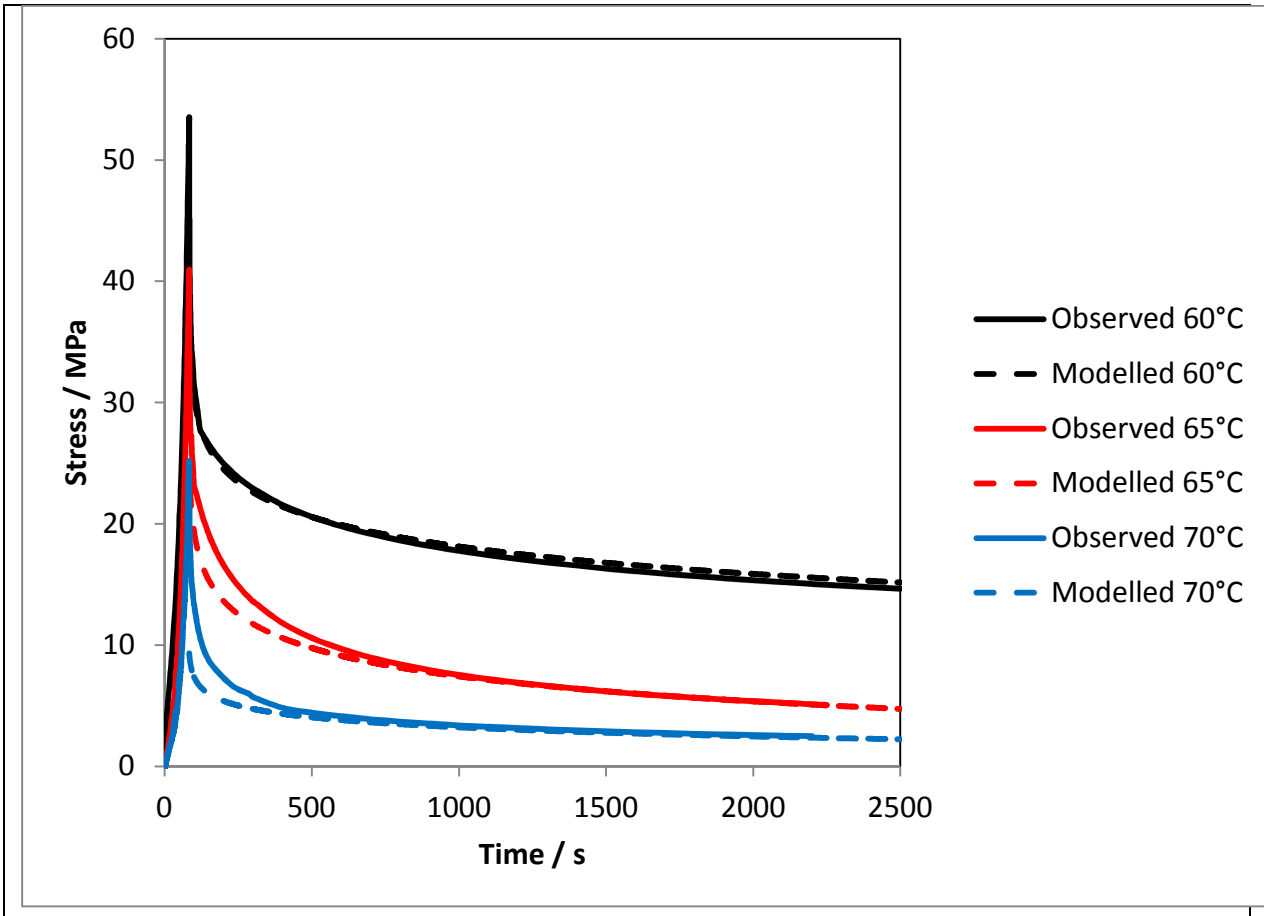

Figure 4(a) Single Eyring process model predictions and experiment at the three test temperatures.

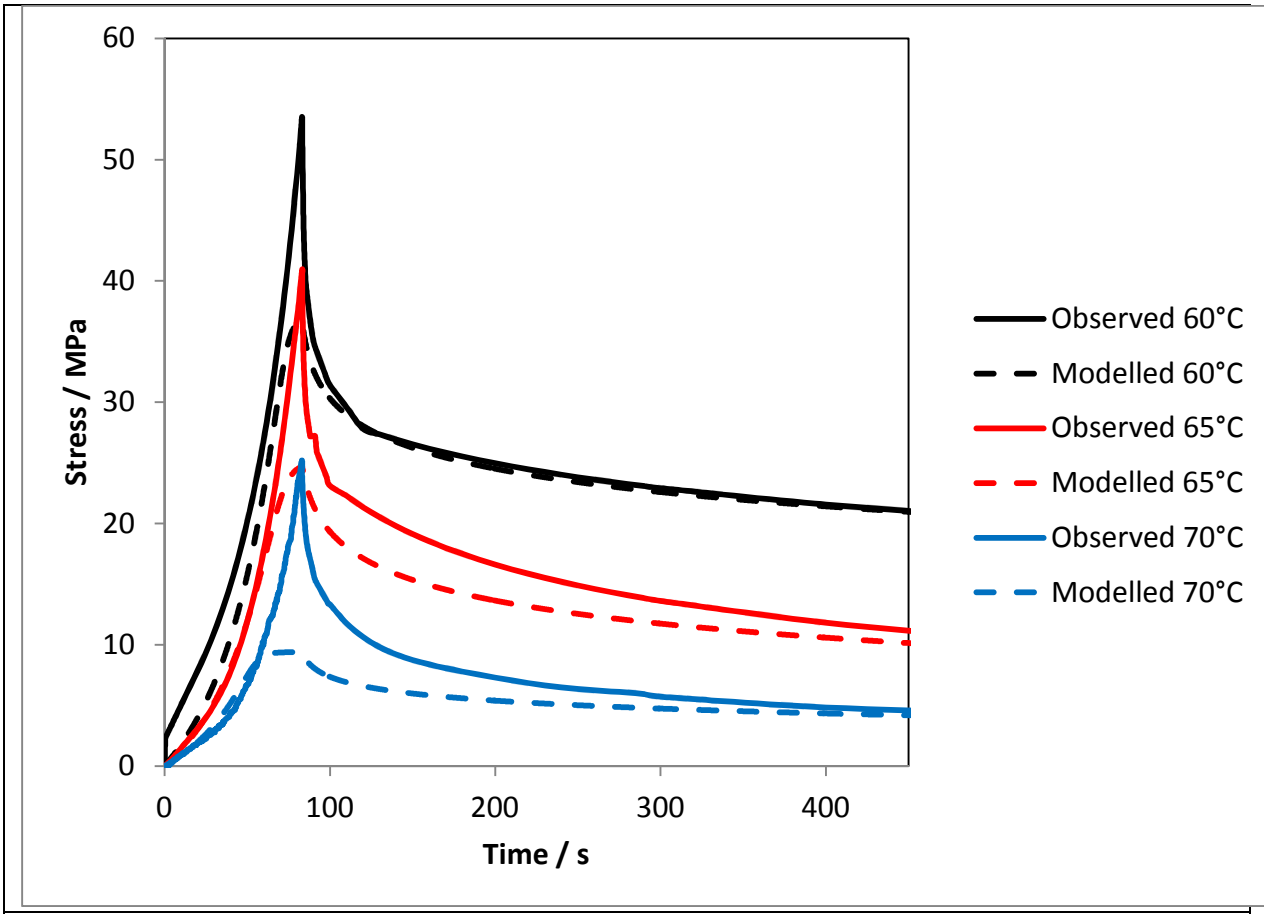

Figure 4(b) Early part of the graph of 4(a).

Stress dip results and implications

The strain histories applied in the stress dip tests are shown in Figure 5, for both small (5% strain, i.e. $\Delta\lambda = 0.05$) and large (10% strain, i.e. $\Delta\lambda = 01.$) strain decrements. Corresponding stresses are shown below for the three temperatures in Figures 7 – 9, alongside the model predictions to be developed in following sections.

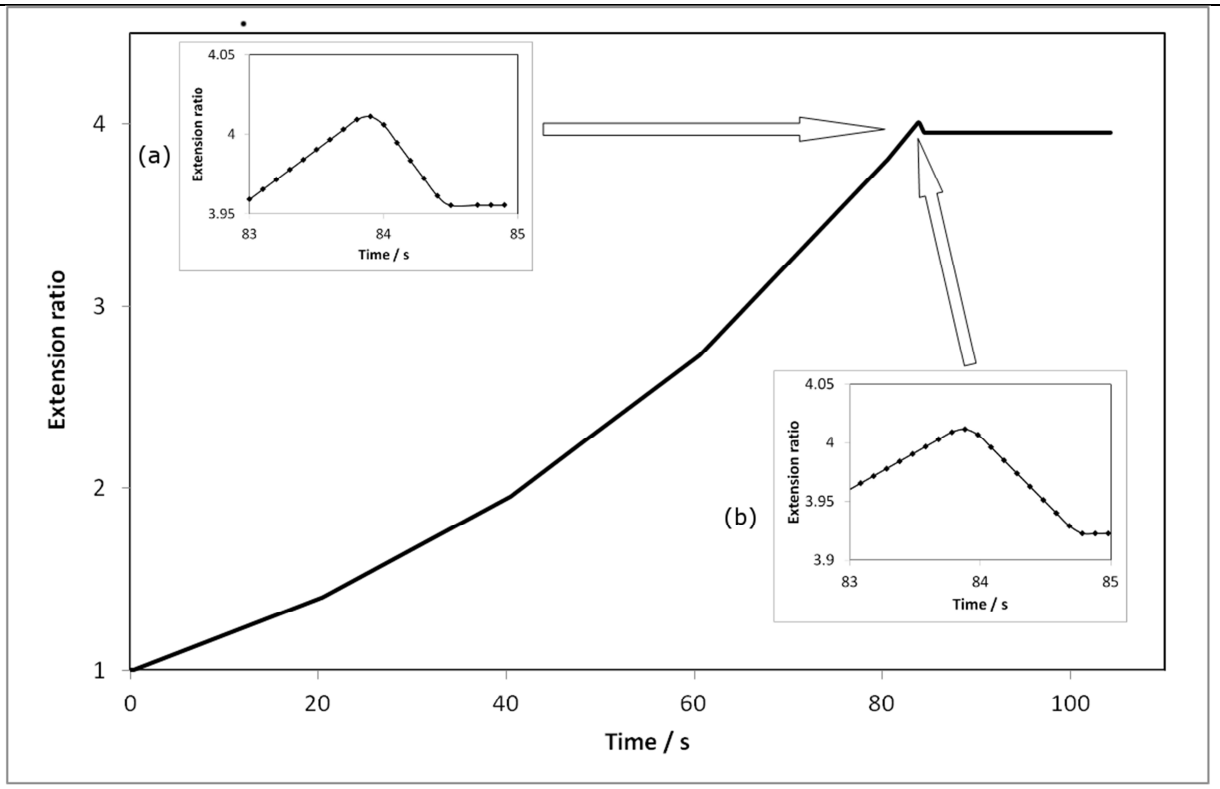

Figure 5. Strain history for stress dip tests: (a) small dip ($\Delta\lambda$ = 0.05); (b) $\Delta\lambda$ = 0.1.

One of the most significant aspects of these tests is the material stiffness associated with the unloading step. Taking the 60°C result with 5% strain dip, we observe a stress drop of 18 MPa. In the time taken for the stress dip (0.6s), the stress relaxation result shows that the stress relaxes by approximately 9 MPa in that time, so we must associate a stress drop of 18 – 9 = 9 MPa with the dip in strain. The stiffness is thus $\frac{\Delta\sigma}{\Delta\lambda} \approx 180$ MPa. To explore the implications of this, suppose it is associated with a neo-Hookean mechanism in which for uniaxial loading the stress is given by

$$\sigma = G\left(\lambda^2 - 1/\lambda\right). \qquad (9)$$

Then, by differentiation the coefficient G is defined in terms of the stiffness as

$$G = \frac{\partial\sigma}{\partial\lambda} / \left(2\lambda + 1/\lambda^2\right) \quad (10).$$

We have already identified an Eyring process from the stress relaxation tests, and established that it does not attain the observed stresses. We require an additional parallel component to model the stress dip behaviour. If we were to associate a neo-Hookean element with this role, the value of the coefficient G from equation (10) gives the stress in equation (9) as ~ 360 MPa at λ = 4, several times greater than the total observed. To exhibit recovery behaviour, the parallel component needs to be viscoelastic, but this calculation shows that the elastic part of the strain associated with it must be very much smaller than the total. This is consistent with the parallel component comprising a stiff elastic element in series with an Eyring process, where it is essential for the Eyring process to have

yielded at an early stage during loading to avoid unrealistically high stress. On this basis we can associate the rate of stress increase as the maximum stress is approached with the plastic mechanism, and the steeper slope on fast unloading with the elastic mechanism in series with the plastic mechanism. For this component to function as observed, the plastic mechanism is prevented by its own hardening from yielding during the strain dip; the yield stress must be higher at large strain than at small strain to allow the observed dip in stress to take place, since the yield stress on loading is observed to be of the order of 2 MPa at 60°C and negligible at higher temperatures.

In this model, the plastic mechanism – the Eyring process – is the main source of strain hardening during loading. This is a major departure from the models, beginning with that of Haward and Thackray [28], in which entropic networks are the sole source of strain hardening. Such networks have featured in polymer constitutive models pursued by many workers subsequently, some of whom have applied the entropic network concept to polymers in their glassy state (for example Smit et al. [30]). This latter course of action, while in some cases producing effective constitutive models, is not justified physically as the entropic chain is by assumption free to assume a wide range of configurations that are not available in the confined glassy state. This issue has been addressed by Mahajan and Basu [31], who, on the basis of molecular simulations of glassy polymer, observed that the glassy and rubbery responses were energetically dissimilar, and concluded that the similarity in stress - strain behaviour between glassy and rubbery systems was not based in physics. Recent work on simulations of glassy polymers has reinforced this view; Hoy and Robbins [32] concluded that, in polymer glasses, strain hardening occurs as a result of an increasing rate of plastic rearrangements that accompanies chain orientation. Macroscopically, this would manifest itself as an increasing dependence of stress on strain rate as orientation increases. Such an effect has been observed by Senden et al. [33], who suggested that it could be modelled by an Eyring activation volume that decreases with strain, in line with similar earlier interpretations [34-36]. However, this approach is only adequate as a model for uniaxial behaviour, as a decrease in activation volume will affect the rate dependence for stretching in all directions, including perpendicularly to the orientation direction. Recognising this, Sweeney et al. [37], who observed an increase in the rate dependence of stress while working on ultra-high molecular weight polyethylene (UHMWPE) in tension, used an Eyring process operating via a flow rule with strain dependent anisotropy. This had the effect of increasing the yield stress along the direction of tensile stretching, leading to a strain-hardening behaviour that was compatible with experimental observations. The same flow rule was also successful in predicting the stress levels along different axes for large multiaxial deformations of both UHMWPE in compression [38] and polypropylene in tension [39]. We shall apply this concept, using a Maxwell-type component consisting of a neo-Hookean element in series with the hardening Eyring process as a parallel arm of the constitutive model.

Constitutive modelling

The following two findings broadly summarise the results so far:

i. Stress relaxation experiments reveal long-term behaviour that can be modelled using an Eyring process.

ii. Stress dip tests reveal extreme degrees of strain stiffening, that cannot be represented by an entropic elastic process. As this stiffening can only occur in the direction of straining, a degree of strain induced anisotropy is implied.

For (i), we have produced an analysis above that uses Guiu-Pratt fitting to help arrive at the material parameters. For (ii), we propose to use an Eyring process as in (i), but one that operates via a flow rule which produces both the strain hardening and the anisotropy; the associated analysis is set out below. By combining together the two types of mechanism associated with (i) and (ii) as components in parallel arms, we shall produce a comprehensive constitutive model that gives a good representation in both the long and short terms. The use of two or more parallel arms gives the potential for tension and compression to coexist, so that the system will also be capable of modelling recovery as in Bonner et al. [17].

Following recent developments [37, 38], we adapt the Hill flow rule [40] such that the Hill coefficients become functions of the total strain. The functions take the form, in principal directions, of the principal extension ratios raised to a power m. In the present case the principal directions remain fixed and coincide with the axes of orthotropy, and we may write for principal directions 1, 2 and 3:

$$\frac{\dot{\lambda}_1^p}{\lambda_1^p} = \dot{e}^p \left[(\lambda_3)^m (\sigma_1 - \sigma_2) + (\lambda_2)^m (\sigma_1 - \sigma_3) \right] / 3\tau$$
$$\frac{\dot{\lambda}_2^p}{\lambda_2^p} = \dot{e}^p \left[(\lambda_1)^m (\sigma_2 - \sigma_3) + (\lambda_3)^m (\sigma_2 - \sigma_1) \right] / 3\tau \quad (11)$$
$$\frac{\dot{\lambda}_3^p}{\lambda_3^p} = \dot{e}^p \left[(\lambda_2)^m (\sigma_3 - \sigma_1) + (\lambda_1)^m (\sigma_3 - \sigma_2) \right] / 3\tau$$

where $\dot{e}^p$ is again the scalar plastic strain rate as in equation (1) that results from the Eyring process

$$\dot{e}^p = \alpha \exp(V_p \bar{\sigma}) \sinh(V_s \tau) \qquad (12).$$

In both equations (11) and (12) τ is the driving stress that differs from the octahedral shear stress of equation (1). The required definition of $\dot{e}^p$ (see Appendix) is maintained provided that

$$\tau = \frac{1}{3} \sqrt{\frac{1}{3} \left[\begin{array}{l} \left\{ (\lambda_3)^m (\sigma_1 - \sigma_2) + (\lambda_2)^m (\sigma_1 - \sigma_3) \right\}^2 \\ + \left\{ (\lambda_1)^m (\sigma_2 - \sigma_3) + (\lambda_3)^m (\sigma_2 - \sigma_1) \right\}^2 \\ + \left\{ (\lambda_2)^m (\sigma_3 - \sigma_1) + (\lambda_1)^m (\sigma_3 - \sigma_2) \right\}^2 \end{array} \right]} \qquad (13).$$

When m = 0, equations (11) revert to the Levy-Mises flow rule and τ reverts to the octahedral shear stress. Otherwise, equations (12) and (13) show that in general the three principal stresses will influence the plastic strain rate to different extents that depend on the level of anisotropy.
We now construct a Maxwell type model similar to that embodied in equations (A12) – (A15) in the Appendix and shown in Figure 1 (a) above. Adopting uniaxial conditions, equations (A12) – (A14) still apply and equation (4) is replaced with the analogue

$$\frac{\dot{\lambda}}{\lambda}=\frac{\dot{\sigma}}{G\left(2(\lambda^{e})^{2}+1/\lambda^{e}\right)}+\alpha\sqrt{2}\exp\left(\frac{v_{p}}{kT}\sigma/3\right)\sinh\left(\sqrt{2}\frac{v_{s}}{kT}\lambda^{-m/2}|\sigma|/3\right) \qquad (14).$$

It is clear that, for tensile stretching and m > 0, the model is strain hardening since the stress, operating via the sinh term, has less influence on the total strain rate as the deformation proceeds. The form of the argument in the sinh function has an effect similar to a strain dependent activation volume. We should note that, in a constitutive model in which the activation volume were a direct function of strain, the level of strain would affect strain hardening equally in all directions and would be unrealistic. By assigning the strain dependence to the flow rule, we ensure that the strain hardening is only influenced for straining along the direction of orientation. The equation (14) is solved numerically in a way similar to that used to solve (4).

From the analysis of stress relaxation we have identified an Eyring process which does not provide sufficient stress at early times. This suggests a strategy of adding a second parallel arm to correct for this. From the stress dip tests we have also seen the need for a very stiff process. It is possible that the second arm and the stiff process are one and the same, in which case the two-arm model of Figure 1(b) would be sufficient. In general, however, we require a constitutive model consisting of three parallel neo-Hookean/Eyring arms, all subject to the same extension ratio λ, as shown in Figure 1(c). Labelling the arms a, b and c, each arm is represented by a copy of equation (14):

$$\frac{\dot{\lambda}}{\lambda}=\frac{\dot{\sigma}_{a}}{G_{a}\left(2(\lambda_{a}^{e})^{2}+1/\lambda_{a}^{e}\right)}+\alpha_{a}\sqrt{2}\exp\left(\frac{v_{pa}}{kT}\sigma_{a}/3\right)\sinh\left(\sqrt{2}\frac{v_{sa}}{kT}\lambda^{-m_{a}/2}|\sigma_{a}|/3\right)$$
$$\frac{\dot{\lambda}}{\lambda}=\frac{\dot{\sigma}_{b}}{G_{b}\left(2(\lambda_{b}^{e})^{2}+1/\lambda_{b}^{e}\right)}+\alpha_{b}\sqrt{2}\exp\left(\frac{v_{pb}}{kT}\sigma_{b}/3\right)\sinh\left(\sqrt{2}\frac{v_{sb}}{kT}\lambda^{-m_{b}/2}|\sigma_{b}|/3\right) \qquad (15).$$
$$\frac{\dot{\lambda}}{\lambda}=\frac{\dot{\sigma}_{c}}{G_{c}\left(2(\lambda_{c}^{e})^{2}+1/\lambda_{c}^{e}\right)}+\alpha_{c}\sqrt{2}\exp\left(\frac{v_{pc}}{kT}\sigma_{c}/3\right)\sinh\left(\sqrt{2}\frac{v_{sc}}{kT}\lambda^{-m_{c}/2}|\sigma_{c}|/3\right)$$

The total stress σ is given by the sum of the stresses in the three arms:

$$\sigma=\sigma_{a}+\sigma_{b}+\sigma_{c} \qquad (16).$$

We identify arm a with the long term process associated with the stress relaxation behaviour and the Eyring parameters summarized in Table 2 above. The proportion of the total stress predicted by this arm can be gauged by observing the 'modelled' curves of Figure 4. The arm b is associated with the stiff strain-hardening process that accounts for a large proportion of the stress during loading and the recovery behaviour. At two of the three temperatures, the fit of the model is improved by introducing the third arm c. The elastic stiffness G_b is initially estimated from the magnitude of the stress dip. The Eyring parameters for the b arm are fitted to ensure an appropriate time scale for the stress recovery process, and the strain hardening exponent m_b is fitted to give the observed shape of the stress-strain curve during loading. In Figures 1(b) and 1(c), the strain-induced anisotropy associated with $m_b=0$ is denoted by the arrowed dashpots. For the a and c processes, the conventional flow rule is retained with $m_a=m_c=0$. G_a and the c arm parameters are adjusted by trial and error to give improvements in the overall representation of the small and large stress dip

experiments and the stress relaxation experiments. The values of the parameters derived in this way are summarized in Table 3, and the associated predictions compared with observation in Figures 6 and 7 for the stress dip tests and in Figure 8 for the stress relaxation tests.

Table 3 Model parameters

Temperature °C	Arm	v_p nm^3	v_s nm^3	α s^{-1}	G MPa	m
60	a	0.256	2.56	7.54×10^{-7}	2.5	0
	b	0.368	3.68	2.4×10^{-2}	450	4.25
65	a	0.243	2.43	3.5×10^{-5}	1.72	0
	b	0.420	4.20	2.4×10^{-2}	270	3.5
	c	0.140	1.40	1.2×10^{-3}	0.6	0
70	a	0.748	7.48	1.3×10^{-5}	0.8	0
	b	1.23	12.3	5.0×10^{-2}	130	5.0
	c	0.237	2.37	1.2×10^{-3}	0.8	0

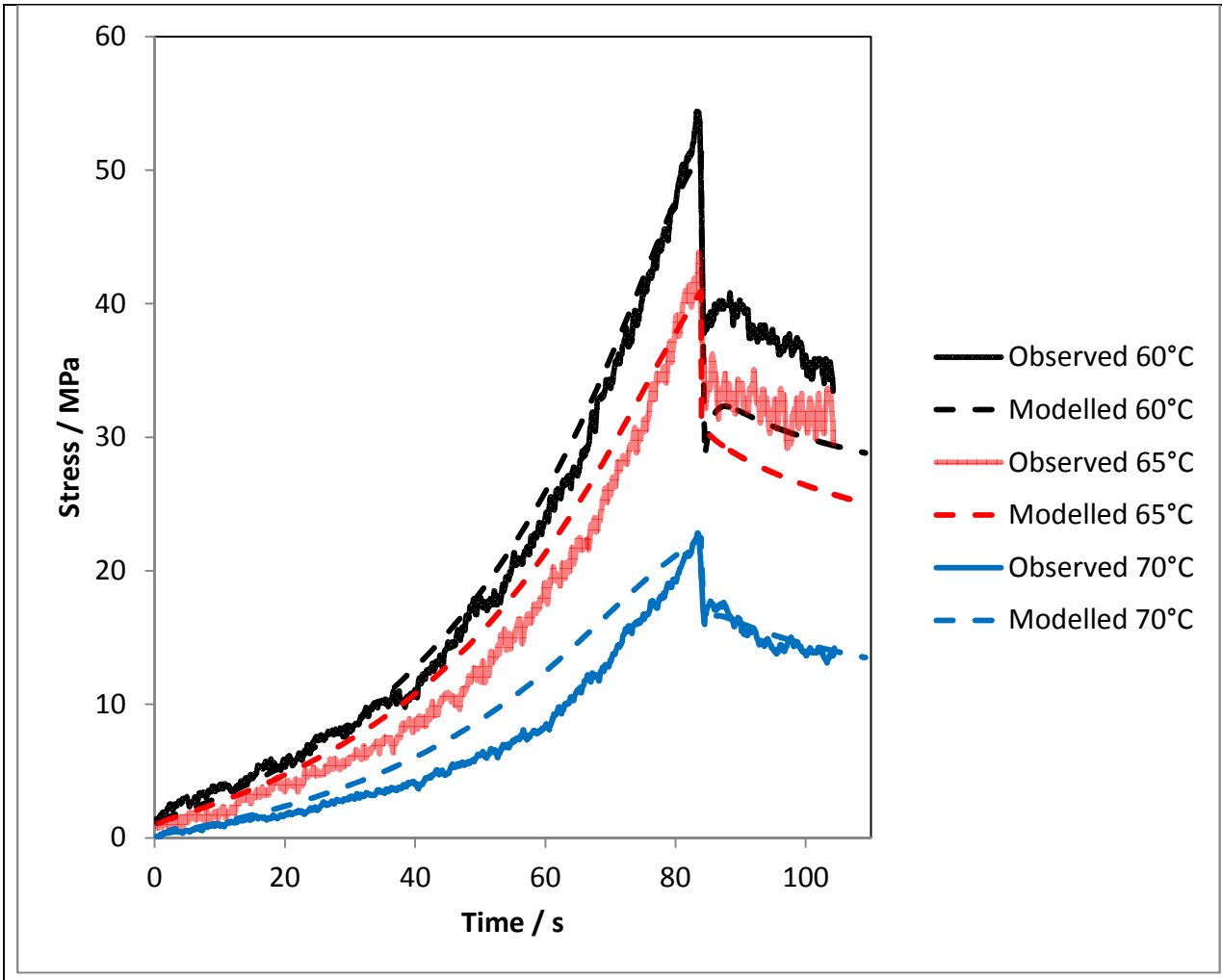

Fig 6 Stress response to small strain dip experiments compared with model predictions.

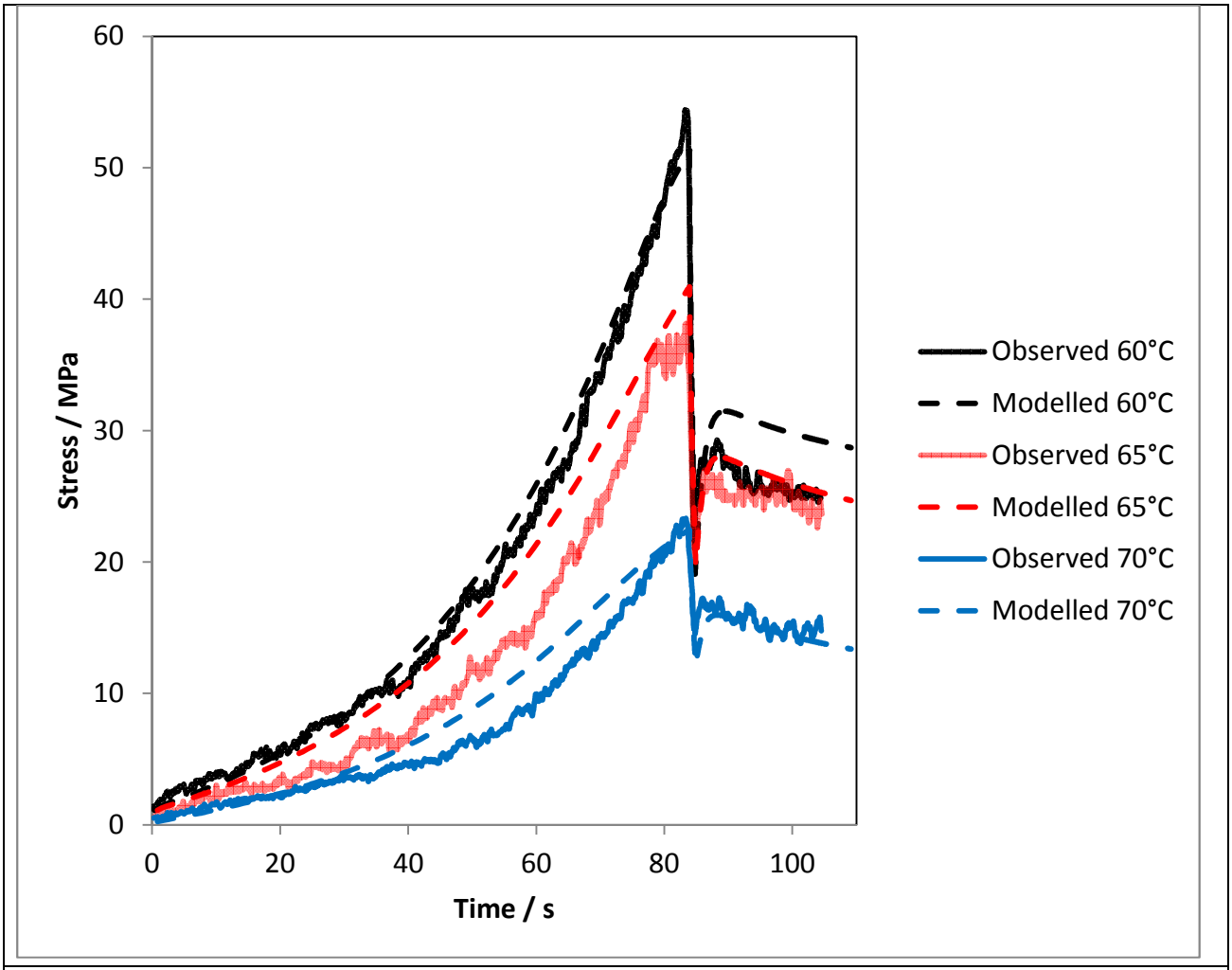

Fig 7 Stress response to large dip experiments compared with model predictions.

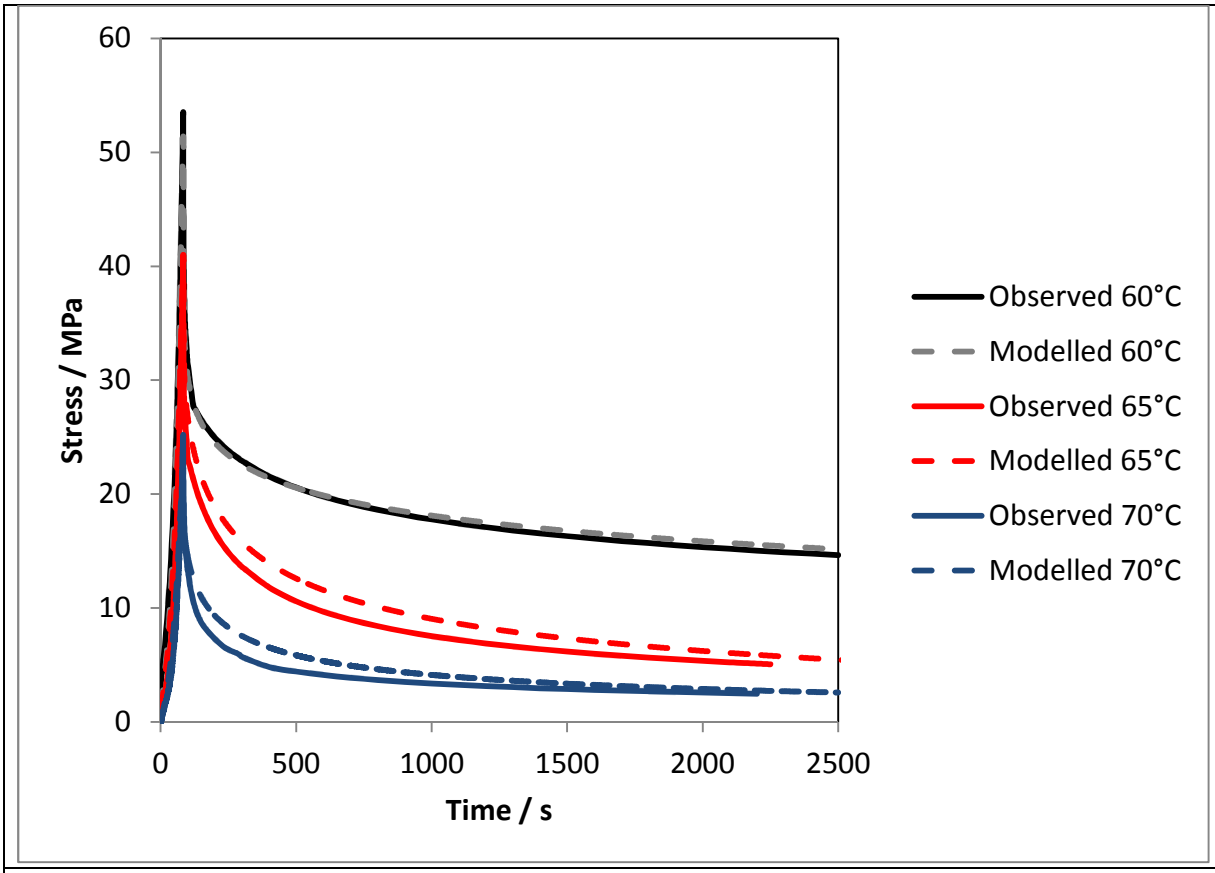

Fig 8(a) Stress responses in stress relaxation experiments compared with model predictions.

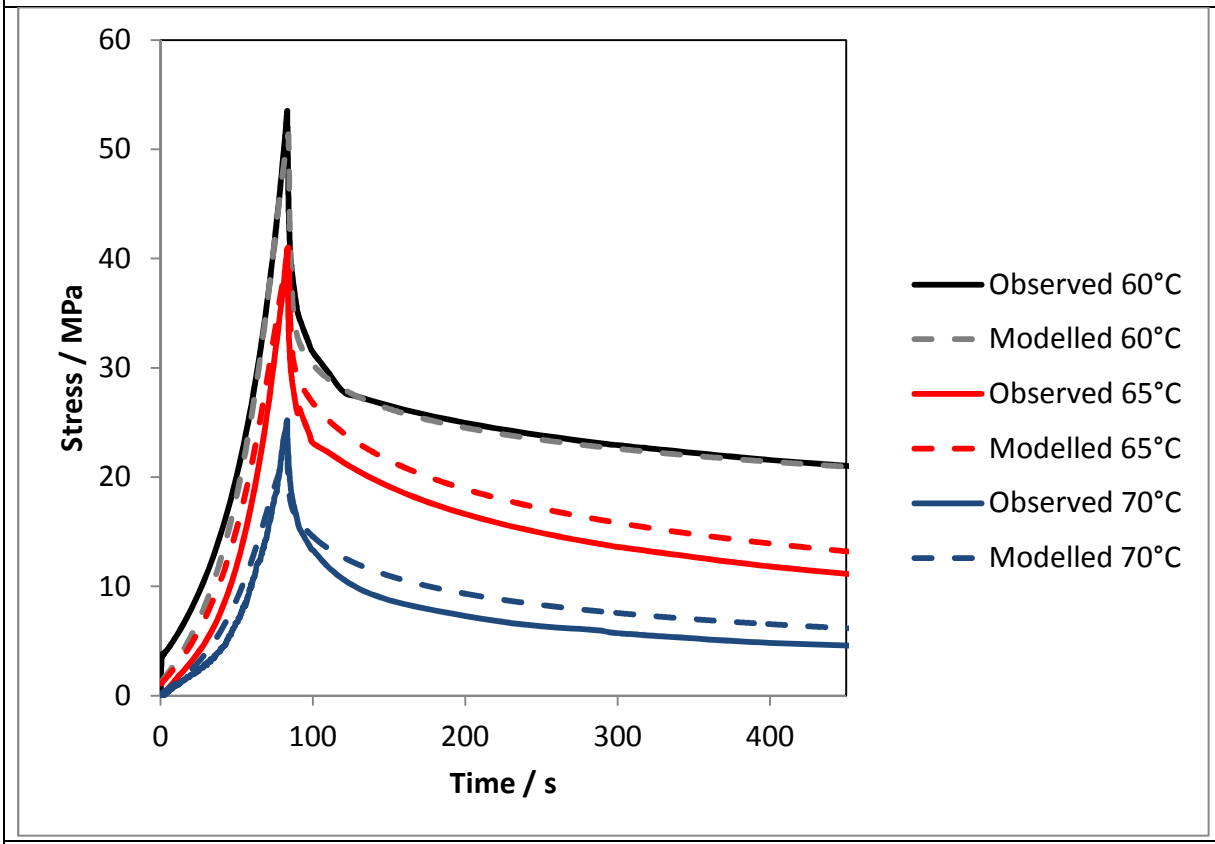

Fig 8(b) Early part of the graph 8(a).

In all cases the model represents loading, stress relaxation and stress recovery at a useful level. The model successfully predicts the distinct levels of stress recovery at low and high strain dips. At 60°C, only two arms - a and b - are necessary, with no significant improvements possible by the addition of a third process. At this temperature, the initial yielding at very low strains predicted for the b process appears to be consistent with the observed stress, whereas at higher temperatures the predicted initial yield is too small to be detected in the experiments reported here. At all three temperatures, the stiff b arm yields at a small strain, so that the elastic strain reaches only around 1% for the total extension ratio of 4.0. This process strain hardens during loading, and accounts for 20-30% of the total stress.

From Table 3, it can be seen that the shear and pressure activation volumes v_s and v_p for arms a and b change little between 60 and 65°C, but undergo large changes between 65 and 70°C, consistent with a glass transition temperature in that range. Activation volumes for polymers of the order of a few nm^3 as seen here are observed for a range of polymers (see for example Haward and Thackray [28]), being considerably greater than the molecular features that they are associated with. Increases in activation volume with temperature have been observed by other workers (see for example Seguela et al. [41]).

Conclusions

A multi-element constitutive model for a shape memory polymer has been successfully developed to represent loading to large tensile deformations, stress relaxation and stress recovery. The model consists of parallel Maxwell arms each comprising neo-Hookean springs and Eyring dashpots.

Guiu-Pratt analysis of the stress relaxation curves is a useful means of deriving Eyring parameters. When these parameters are set to define the Eyring process in a single Maxwell arm, the resulting model (Figure 1(a)) yields at a stress lower than that attained during loading, but gives good predictions for longer times. This highlights the need for one or more additional parallel arms to provide a realistic initial response.

Stress dip tests show a very stiff response on unloading. This phenomenon is modelled by introducing an essential basic component in the form of an Eyring process that operates via a flow rule that introduces strain-induced anisotropy. For this process, the dependence of stress on strain rate in the stretching direction increases in strength as the strain increases. As a result, the process shows strain hardening after yield, and when included in series with a neo-Hookean spring it forms a single-arm strain hardening model. In this Maxwell type model the strain hardening is driven by the extension of the Eyring process. Hence, we have a source for strain-hardening behaviour that is not attributable to entropic elasticity, a feature consistent with the polymer behaviour predicted by molecular dynamics simulation. Also, with this process the yield stress is higher at higher strain, so that it can yield at a low strain and, after the imposition of a large strain, then be unloaded through a stress decrement greater than the initial yield. This enables the very stiff mechanism observed when unloading through a small strain dip to be modelled with a single process.

To accommodate both the long term response in stress relaxation and the stiff response during stress dips, a two-arm model is necessary (see Figure 1(b)). If the stiff mechanism in arm b of this model also provides the stress required for the initial response, then the two-armed model of 1(b) is sufficient; this is the case at 60°C. At the other temperatures, a third arm becomes necessary, resulting in the model of Figure 1(c).

The level of understanding achieved will allow the development of accurate finite element analyses of shape memory components. This will enable the evaluation of a number of factors useful to the design process. These factors include the evolution during recovery of the component shape; the boundary forces generated at the interface of the component with the surrounding tissue; the recovery time; and the required duration of heating during the thermal triggering process.

References

[1] Ratner D., Karger-Kocsis J.,2008. Recent Advances in shape memory polymers and composites: a review. J. Mater. Sci. 43, 254-269.

[2 Lendlein A., Behl M., 2009. Shape-Memory Polymers for Biomedical Applications , in: Vincenzini, P., Darrigo, G. (Eds.) Smart Materials & Micro/Nanosystems. Vol. 54 of Advances in Science and Technology, Trans Tech Publications, Switzerland pp. 96 – 102.

[3] Wache H.M., Tartakowska D.J., Hentrich A., Wagner M.H., 2003. Development of a polymer stent with shape memory effect as a drug delivery system. J Mater Sci: Materials in Medicine. 14, 109-112.

[4] Venkatraman SS, Tan LP, Joso JFD, Boey YCF, Wang X. Biodegradable stents with elastic memory. Biomaterials 2006; 27:1573-1578.

[5] Xue L, Dai S, Li Z. Biodegradable shape-memory block co-polymers for fast self-expandable stents. Biomaterials 2010; 31:8132-8140.

[6] Yakacki CM, Shandas R, Lanning C, Rech B, Eckstein A, Gall K. Unconstrained recovery characterization of shape-memory polymer networks for cardiovascular applications Biomaterials 28 2255-2263 2007.

[7] Neuss S, Blomenkamp I, Stainforth R, Boltersdorf D, Jansen M, Butz N, Perez-Bouza A, Knüchel R. The use of a shape-memory poly(ε-caprolactone)dimethacrylate network as a tissue engineering scaffold. Biomaterials 2009;30: 1697-1705.

[8] Hun-Sik Kim, Byung Hyun Park, Jae Hoon Choi, Jin-San Yoon Mechanical Properties and Thermal Stability of Poly(L-lactide)/Calcium Carbonate Composites Journal of Applied Polymer Science, Vol. 109, 3087–3092 2008.

[9] Vitalija BETINGYTĖ, Kristina ŽUKIENĖ, Virginija JANKAUSKAITĖ, Daiva MILAŠIENĖ, Kazys Vytautas MICKUS, Ada GULBINIENĖ, Influence of Calcium Carbonate Fillers on the Properties of Recycled Poly(ε-caprolactone) Based Thermoplastic Polyurethane ISSN 1392–1320 MATERIALS SCIENCE (MEDŽIAGOTYRA). Vol. 18, No. 3. 243-249 2012.

[10] Ken Gall, Christopher M. Yakacki, Yiping Liu, Robin Shandas, Nick Willett, Kristi S. Anseth Thermomechanics of the shape memory effect in polymers for biomedical applications. J Biomed Mater Res 73A: 339–348, 2005.

[11] Brown M, Montes De Oca Balderas H, Howling G, Rains J, Rose J, Hall M, Chivers RA, Marsh A. Systems and methods for installing and removing an expandable polymer. Patent publication number WO/2008/112880 2008.

[12] Montes De Oca Balderas H, Brown M, Thompson A, Howling G. Fixation device. Patent publication number WO/2008/129241 2008.

[13] Montes De Oca Balderas H, Brown M, Bonner MJ, Ward IM, Hall M, Rose J, Bettenga M. Orientated polymeric devices. Patent publication number WO/2008/131221 2008.

[14] H. DERAMOND, N. T. WRIGHT, S. M. BELKOFF Temperature Elevation Caused by Bone Cement Polymerization During Vertebroplasty. Bone Vol. 25, No. 2, 17S–21S Supplement August 1999.

[15] Nguyen TD, Yakacki CM, Brahmbhatt PD, Chambers ML. Modeling the Relaxation Mechanisms of Amorphous Shape Memory Polymers. Advanced Materials 2010;22:3411-3423.

[16] Fotheringham DG, Cherry BW. The role of recovery forces in the deformation of linear polyethylene. J Mater Sci 1978;13:951-964.
[17] Bonner M, Montes de Oca Balderas H, Brown M, Ward IM. A novel approach to predict the recovery time of shape memory polymers. Polymer 2010;51:1432-1436.
[18] Guiu F., Pratt P.L., 1964, Stress relaxation and the plastic deformation of solids. Phys Status Solidi 1964;6:111-120.
[19] Halsey G, White HJ, Eyring H. Mechanical properties of textiles I. Text Res J 1945;15:295-311.
[20] Truss RW Duckett RA Ward IM. Effect of hydrostatic pressure on the yield and fracture of polyethylene in torsion. J Mater Sci 1981;16:1689-1699.
[21] Buckley CP, Jones DC. Glass-rubber constitutive model for amorphous polymers near the glass transition. Polymer 1995;36:3301-3312.
[22] Spathis G, Kontou E. Nonlinear viscoelastic and viscoplastic response of glassy polymers. Polym. Eng. Sci. 2001; 41:1337–1344.
[23] Klompen ETJ, Engels TAP, van Breemen LCA, Schreurs PJG, Govaert LE, Meijer HEH. Quantitative Prediction of Long-Term Failure of Polycarbonate. Macromolecules 2005;38:7009-7017.
[24] Bauwens-Crowet C, Bauwens J-C. The temperature dependence of yield of polycarbonate in uniaxial compression and tensile tests. J Mater Sci 1972;7:176-183.
[25] Nazarenko S, Bensason S, Hiltner, A, Baer E. The effect of pressure on the necking of polycarbonate. Polymer 1994;35:3883-3892.
[26] Joseph SH, Duckett RA. Effects of pressure on the non-linear viscoelastic behaviour of polymers:1. Polypropylene. Polymer 1978;19:837-849.
[27] Naz S, Sweeney J, Coates PD. Analysis of the essential work of fracture method as applied to UHMWPE. J Mater Sci 2010;45,:448-459.
[28] Haward RN, Thackray G. The use of a mathematical model to describe isothermal stress-strain curves in glassy thermoplastics. Proc Roy Soc A 1968;302:453-472.
[29] Srutz SJ, Brower SC,Hayden LM. Temperature dependence of the activation volume in a nonlinear optical polymer: evidence for chromophore reorientation induced by sub-T_g relaxations. J Polym Sci B Physics 1998; 36:901-911.
[30] Smit RJM, Brekelmans WAM, Meijer HEH. Prediction of large-strain mechanical response of heterogeneous polymer systems: local and global deformation behaviour of a representative volume element of voided polycarbonate. J Mech Phys Solids 1999; 47:201-221.
[31] Mahajan DK, Basu S. Investigations into the applicability of rubber elastic analogy to hardening in glassy polymers. Modelling and simulation in materials science and engineering 2010;18:025001.
[32] Hoy RS, Robbins MO. Strain hardening in bidisperse polymer glasses: Separating the roles of chain orientation and interchain entanglement. J Chem Phys 2009; 131:244901.
[33] Senden DJA, van Dommelen JAW, Govaert LE. Strain Hardening and Its Relation to Bauschinger Effects in Oriented Polymers. Journal of Polymer Science: Part B: Polymer Physics 2010;48:1483-1494.
[34] Hope, PS Ward IM, Gibson AG. The Hydrostatic Extrusion of Polymethylmethacrylate. J Mater Sci 1980;15:2207-2220.
[35] Hope PS, Ward IM. An Activated Rate Theory Approach to the Hydrostatic Extrusion of Polymers. J Mater Sci 1981;16:1511-1521.
[36] Ward, IM. The role of molecular networks and thermally activated processes in the deformation behavior of polymers. Polym Eng Sci 1984;24:724-736.
[37] Sweeney J, Naz S, Coates PD. Modeling the tensile behavior of UHMWPE with a novel flow rule. J Appl Polym Sci 2010;121:2936-2944.

[38] Sweeney J, Naz S and Coates PD 2009 Viscoplastic Constitutive Modeling of Polymers—Flow Rules and the Plane Strain Response, J Appl Polym Sci 2009;111:1190-1198.
[39] Sweeney J, O'Connor CPJ, Spencer PE, Pua H, Caton-Rose P, Martin PJ. A material model for multiaxial stretching and stress relaxation of polypropylene under process conditions Mechanics of Materials 2012; 54:55-69.
[40] Hill R. The mathematical theory of plasticity. Oxford: Oxford University Press; 1985.
[41] Seguela R, Staniek E, Escaig B, Fillon B. Plastic deformation of polypropylene in relation to crystalline structure. J Appl Polym Sci 1991; 71:1873-1885.

Appendix: Analysis of single Maxwell arrangement for uniaxial stretching

For the Maxwell model of Figure 1(a), the plastic strain rate $\dot{e}^p$ in the Eyring process is given by

$$\dot{e}^p = \alpha \exp\left(\frac{v_p}{kT}\bar{\sigma}\right)\sinh\left(\frac{v_s}{kT}\tau_{oct}\right) \qquad (A1)$$

for a stress tensor with octahedral shear stress τ_{oct} and mean value $\bar{\sigma}$. α is a constant pre-exponential factor and v_p and v_s are the pressure and shear activation volumes v_p and v_s respectively, with k Boltzmann's constant and T the absolute temperature. In the following analysis for uniaxial conditions the principal directions of stress and strain remain coincident and along the global 1-2-3 axis set. For principal stresses σ_1, σ_2 and σ_3 the mean stress is given by

$$\bar{\sigma} = (\sigma_1 + \sigma_2 + \sigma_3)/3 \quad (A2)$$

and the octahedral shear stress is

$$\tau_{oct} = \frac{1}{3}\left((\sigma_1 - \sigma_2)^2 + (\sigma_2 - \sigma_3)^2 + (\sigma_3 - \sigma_1)^2\right)^{1/2} \quad (A3).$$

The plastic strain rate tensor $\mathbf{L^p}$, given in terms of principal plastic extension ratios λ_1^p, λ_2^p and λ_3^p and their rates $\dot{\lambda}_1^p$, $\dot{\lambda}_2^p$ and $\dot{\lambda}_3^p$ is given by

$$\mathbf{L^p} = \begin{pmatrix} \frac{\dot{\lambda}_1^p}{\lambda_1^p} & 0 & 0 \\ 0 & \frac{\dot{\lambda}_2^p}{\lambda_2^p} & 0 \\ 0 & 0 & \frac{\dot{\lambda}_3^p}{\lambda_3^p} \end{pmatrix} \quad (A4)$$

and the scalar plastic strain rate in equation (A1) is then

$$\dot{e}^p = \sqrt{\frac{1}{3}\mathbf{L^p} : \mathbf{L^p}} \quad (A5).$$

Since the plastic strains are assumed to be incompressible, for uniaxial stretching along 1,

$$\lambda_2^p = \lambda_3^p = \left(\lambda_1^p\right)^{-1/2} \qquad \text{(A6)}$$

and

$$\frac{\dot{\lambda}_2^p}{\lambda_2^p} = \frac{\dot{\lambda}_3^p}{\lambda_3^p} = -\frac{\dot{\lambda}_1^p}{2\lambda_1^p} \qquad \text{(A7).}$$

Also,

$$\sigma_2 = \sigma_3 = 0 \qquad \text{(A8).}$$

Now, writing $\sigma = \sigma_1$ and $\lambda_1^p = \lambda^p$ and using equations (A2) – (A7), equation (A1) becomes

$$\left|\frac{\dot{\lambda}^p}{\lambda^p}\right| = \alpha\sqrt{2}\exp\left(\frac{v_p}{kT}\sigma/3\right)\sinh\left(\sqrt{2}\frac{v_s}{kT}|\sigma|/3\right) \qquad \text{(A9).}$$

To obtain a Guiu-Pratt relation we make the assumption that the argument in the sinh function is large so that $\sinh(x) \simeq \exp(x)/2$. Then for $\sigma > 0$ equation (A9) becomes

$$\left|\frac{\dot{\lambda}^p}{\lambda^p}\right| = \frac{\alpha}{\sqrt{2}}\exp\left(\frac{v}{kT}\sigma\right) \qquad \text{(A10)}$$

where

$$v = \left(v_p + \sqrt{2}v_s\right)/3 \qquad \text{(A11).}$$

For uniaxial conditions along the 1 axis with elastic extension ratio λ^e, the stress along the 1 axis for the incompressible neo-Hookean model is given by

$$\sigma = G\left((\lambda^e)^2 - 1/\lambda^e\right) \qquad \text{(A12).}$$

where G is a material constant. For the series model with a total extension ratio λ,

$$\lambda = \lambda^e\lambda^p \qquad \text{(A13)}$$

and

$$\frac{\dot{\lambda}}{\lambda} = \frac{\dot{\lambda}^e}{\lambda^e} + \frac{\dot{\lambda}^p}{\lambda^p} \qquad \text{(A14).}$$

Using the time derivative of equation (A12) and equation (A9) for positive strain rate, equation (A14) becomes

$$\frac{\dot{\lambda}}{\lambda}=\frac{\dot{\sigma}}{G\left(2(\lambda^e)^2+1/\lambda^e\right)}+\alpha\sqrt{2}\exp\left(\frac{v_p}{kT}\sigma/3\right)\sinh\left(\sqrt{2}\frac{v_s}{kT}\sigma/3\right) \quad \text{(A15)}$$

with a simplified version using equation (10)

$$\frac{\dot{\lambda}}{\lambda}=\frac{\dot{\sigma}}{G\left(2(\lambda^e)^2+1/\lambda^e\right)}+\frac{\alpha}{\sqrt{2}}\exp\left(\frac{v}{kT}\sigma\right) \quad \text{(A16).}$$

For stress relaxation, $\dot{\lambda}=0$ in (A16) gives the differential equation

$$\frac{\dot{\sigma}}{G\left(2(\lambda^e)^2+1/\lambda^e\right)}+\frac{\alpha}{\sqrt{2}}\exp\left(\frac{v}{kT}\sigma\right)=0 \quad \text{(A17).}$$

A Guiu-Pratt type solution of equation (A17) is possible only if it is assumed that the factor $\left(2(\lambda^e)^2+1/\lambda^e\right)$ is constant. This is approximately true for slowly changing stress. We shall use the solution to estimate Eyring parameters, taking due regard of this limitation. Under this condition the solution for the stress at time t constant strain is given by

$$\sigma(t_0)-\sigma(t)=\frac{kT}{v}\ln(1+(t-t_0)/c) \quad \text{(A18)}$$

where $t > t_0$ with t_0 a fixed time, often equated to $t_0 = 0$ at the start of the stress relaxation. c is given by

$$c=\frac{kT\sqrt{2}}{\alpha v G\left(2(\lambda^e)^2+1/\lambda^e\right)}\exp\left(-\frac{v}{kT}\sigma(t_0)\right) \quad \text{(A19).}$$

For the applications in this paper, equation (A18) is fitted to stress relaxation curves to estimate V and α, and stresses during loading are calculated by a time-stepping numerical implementation of equation (A15) in which derivatives are replaced by forward differences. In this procedure, stress σ is substituted by an expression in λ and λ_p using equations (A12) and (A13) and the resulting equation (A15) solved for λ_p.